Seismic response of poro-elastic seabed and composite breakwater under strong earthquake loading
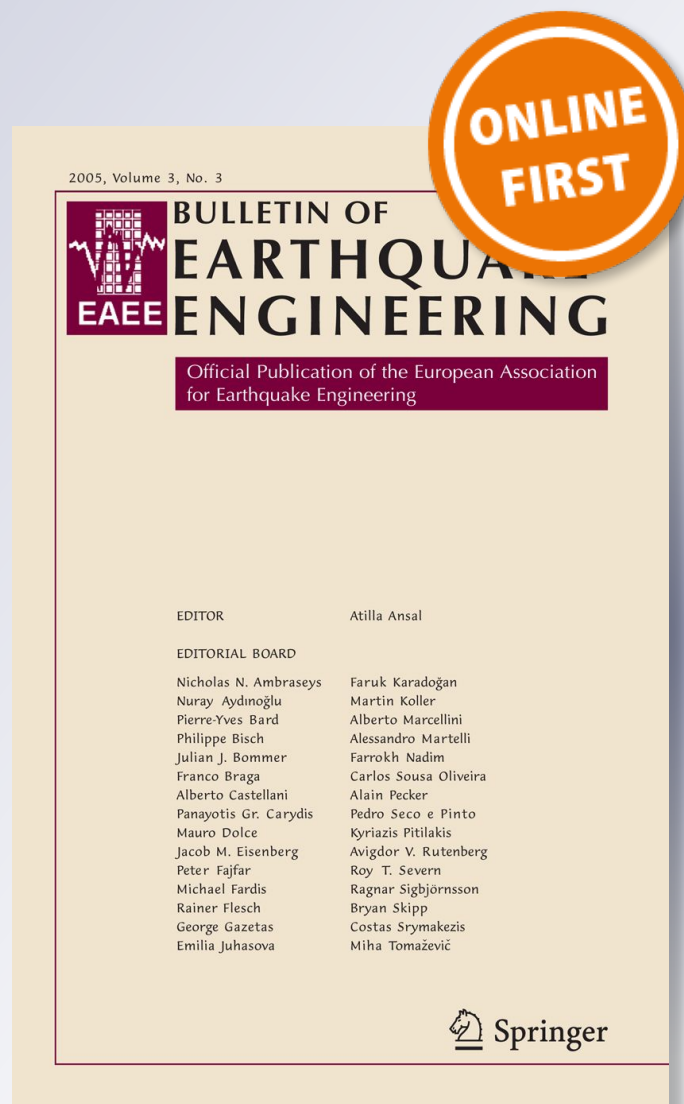
Jianhong Ye

Springer

Springer

ORIGINAL RESEARCH PAPER

Seismic response of poro-elastic seabed and composite breakwater under strong earthquake loading

Jianhong Ye

Abstract   The marine structures in offshore area, such as composite breakwater, are generally vulnerable to the strong seismic wave propagating through their seabed foundation. There are a lot of failure examples during the strong earthquake events in the world in the past 20 years. However, attention given to the seismic response of marine structures under strong seismic wave is limited. In this study, taking the dynamic Biot's equation "$u - p$" as the governing equation for porous seabed foundation, the seismic response of a composite breakwater and its porous seabed foundation under the seismic wave recorded in the Japan 311 off the pacific coast of Tohoku earthquake ($M_L = 9.0$) is investigated using a FEM numerical model. The numerical results indicate that the seismic response of composite breakwater is very strong in the earthquake process. The amplification of the input seismic wave occurs both in seabed foundation and composite breakwater; and this amplification is positively related to the buried depth of points. The horizontal seismic response is much strong than the vertical seismic response. The seismic wave induced excess pore pressure and effective stresses in seabed foundation vibrates; the vibration amplitude is also positively related to the buried depth of points. Under strong seismic loading, the surface region of seabed foundation could liquefy. The parametric study shows that the young's modulus of seabed foundation has significant effect on the seismic response of composite breakwater.

Keywords   Seismic response · Biot's theory · Composite breakwater · Seabed foundation · Poro-elasticity · Consolidation · Japan 311 Tohoku earthquake

J. Ye (✉)
Key Laboratory of Engineering Geomechanics, Institute of Geology and Geophysics,
Chinese Academy of Sciences, Beijing 100029, China
e-mail: yejianhongcas@gmail.com

J. Ye
Division of Civil Engineering, University of Dundee, Dundee DD1 4HN, UK

 Springer

1 Introduction

In recent two decades, more and more marine structures, such as breakwater, oil platform and turbines are constructed on seabed in offshore area. The stability of these marine structures after construction under the environmental loading is the main concern for the coastal engineers involved in the design work. As a kind of marine structure, the composite breakwater are widely adopted to protect the port and harbor in the world, especially in Japan and Spain. Generally, there are two types of environmental loading in offshore area. One is the ocean wave, another is the probable earthquake. The ocean wave is the conventional loading for all marine structures. The effect of ocean wave loading on the stability of marine structures has been investigated widely. However, as the second type of environmental loading—seismic wave, little attention and investigation has been paid and conducted in the previous literatures. At present, the seismic coefficient method based on the static analysis is widely adopted in anti-seismic design for breakwater in engineering practice. The seismic loading is not a conventional loading for breakwaters; and the strong earthquake may not occur at the zone nearby the foundation site of breakwater in its usage life. However, once the earthquake occurs at nearby place, the damage to these marine structures would be devastating. For example, the failure of marine structure in Los Angeles (USA) in 1994, Kobe (Japan) in 1995, Kocaeli (Turkey) in 1999; Athens (Greece) in 1999 and Sumatra (Indonesia) in 2003. Some literatures are available about the earthquake induced failure of marine structures (Memos and Protonotarios 1993; Iai and Kameoka 1993; Sugano et al. 1999; Sumer et al. 2002; Yuksel et al. 2004; Katopodi and Iosifidou 2004). Therefore, besides the wave loading, the seismic loading should be considered for some important structures built in active seismic zone, for example, the east coast of Japan. More sophisticated seismic response analysis is needed, rather than adopting the quasi-static design method.

The dynamic response of breakwater under wave loading has been investigated extensively in the previous three decades. A great number of results and models are available in previous literatures. A brief review on this tropic can be found in Young et al. (2009). At present, the experimental and numerical investigation on the seismic response of a composite breakwater under earthquake loading are still limited. Only few literatures are available. Among them, Yuksel et al. (2004) analyzed the seismic wave induced deformation of breakwaters at the Eregli Fishery port during 1999 Koceali Turkey earthquake using the material properties obtained from the field sites. Kiara et al. (2004) and Memos et al. (2000) conducted a series of experimental test to investigate the seismic response and stability of a rubble mound breakwater under seismic wave loading on shaking table. In their experiment, they found the response acceleration is negatively related to the buried depth in sandy bed; and the sandy bed is the dominant role for the breakwater failure. The numerical study was also performed in their study. The dynamic water pressure acting on outer surface of rubble mound breakwater was taken into consideration based on the Westerggard's equation (Westergaard 1933). Similar shaking table tests were also conducted by Ozaki and Nagao (2004). Based on the work of Kiara et al. (2004) and Memos et al. (2000, 2003) further numerically investigated the seismic response analysis of rubble mound breakwater using a coupled model, in which the boundary element method is used to solve the fluid domain. The coupling is implemented through the iteration and the continuity of displacement at the interface between the rubble mound breakwater and the water. However, the input motion is only harmonic shaking, not a real seismic wave. Jafarian et al. (2010) adopts the finite difference program FLAC to estimate the permenant displacement of a rubble mound breakwater on sandy bed under seismic wave loading. In their study, the Mohr–Coulomb constitutive model (Elastic-perfectly plastic) and the pore pressure built-up model proposed by Byme (1991) are used. Obviously, the soil

particles and pore water are not coupled. Recently, Cihan and Yuksel (2011) also experimentally and numerically investigates the deformation of rubble mound breakwater under horizontal harmonic vibration. In their experimental tests, it is found that the rubble mound breakwater would collapse under strong vibration. In their numerical study, the FEM software PLAXIS is adopted. The horizontal harmonic vibration is input at the based on breakwater. However, the pore water in rubble mound breakwater, and the dynamic pressure acting on the lateral sides of breakwater induced by the vibration of breakwater are both not considered.

Chen (2000) and Chen and Huang (2002) developed a coupled model to estimate the seismic wave induced hydrodynamic force on sea wall or caisson wall. Recently, similar work is also conducted adopting commercial software ADINA (Arablouei et al. 2011). Mohajeri et al. (2004) experimentally studied the earthquake induced sliding displacement of caisson wall on shaking table. All the above mentioned investigations are all focused on the rubble mound breakwater and caisson wall or sea wall. At present, to the author's knowledge, there is no literatures available on the topic about the numerical investigation of the seismic response of a composite breakwater built on porous seabed foundation.

In this study, taking the dynamic Biot's equation "$u - p$" proposed by Zienkiewicz et al. (1980) as the governing equation, in which the effect of acceleration of soil and pore water are considered, a 2D FEM numerical model (PORO-WSSI II) is developed based on SWAN-DYNE (Chan 1988; Zienkiewicz et al. 1999). The water wave induced dynamic pressure or hydrostatic water pressure acting on seabed and outer surface of marine structures can be applied in earthquake analysis in PORO-WSSI II. By adopting the developed 2D FEM numerical model, the seismic response of a composite breakwater resting on a poro-elastic seabed under a strong earthquake loading is investigated.

2 Governing equation

It has been commonly known that soil is a multi-phase material consisting of soil particles, water and trapped air. In the soil mixture, the soil particles form the skeleton; the water and the air fill the void of skeleton. Therefore, soil is a three-phase porous material, rather than a continuous medium. In this study, the dynamic Biot's equation known as "$u - p$" approximation proposed by Zienkiewicz et al. (1980) are used to govern the dynamic response of the porous medium under wave loading, in which the relative displacements of pore fluid to soil particles are ignored, but the acceleration of the pore water and soil particles are included:

$$\frac{\partial \sigma'_x}{\partial x} + \frac{\partial \tau_{xz}}{\partial z} = -\frac{\partial p}{\partial x} + \rho \frac{\partial^2 u}{\partial t^2}, \tag{1}$$

$$\frac{\partial \tau_{xz}}{\partial x} + \frac{\partial \sigma'_z}{\partial z} + \rho g = -\frac{\partial p}{\partial z} + \rho \frac{\partial^2 v}{\partial t^2}, \tag{2}$$

$$k\nabla^2 p - \gamma_w n\beta \frac{\partial p}{\partial t} + k\rho_f \frac{\partial^2 \epsilon}{\partial t^2} = \gamma_w \frac{\partial \epsilon}{\partial t}, \tag{3}$$

where $(u, v) =$ the soil displacements in the horizontal and vertical directions, respectively; $n =$ soil porosity; σ'_x and $\sigma'_z =$ effective normal stresses in the horizontal and vertical directions, respectively; $\tau_{xz} =$ shear stress; $p =$ the pore water pressure; $\rho = \rho_f n + \rho_s(1 - n)$ is the average density of porous seabed; $\rho_f =$ the fluid density ; $\rho_s =$ solid density; $k =$ the Darcy's permeability; $g =$ the gravitational acceleration, γ_ω is unit weight and ϵ is the volumetric strain. In Eq. (3), the compressibility of pore fluid (β) and the volume strain (ϵ) are defined as

$$\beta = \left(\frac{1}{K_f} + \frac{1 - S_r}{p_{w0}} \right), \quad \text{and} \quad \epsilon = \frac{\partial u}{\partial x} + \frac{\partial v}{\partial z}, \tag{4}$$

where S_r = the degree of saturation of seabed, p_{w0} = the absolute static pressure and K_f = the bulk modulus of pore water.

3 Numerical model

The finite element method is used to solve the governing equations (1)–(3). For dynamic problems, the spatial discretization and temporal discretization have to be performed for the above three governing equations.

Spatial discretization The spatial discretization involves the variables $\mathbf{u}$ and $\mathbf{p}$ are replaced by suitable shape functions in the governing equations.

$$\mathbf{u} = \sum N_i^u u_i = \mathbf{N^u \bar{u}} \tag{5}$$

$$\mathbf{p} = \sum N_i^p p_i = \mathbf{N^p \bar{p}} \tag{6}$$

where $\mathbf{u}$ and $\mathbf{p}$ are the displacement vector of soil and the pore pressure. The $\mathbf{\bar{u}}$ and $\mathbf{\bar{p}}$ are the vectors of node displacement and pore pressure. The $\mathbf{N^u}$ and $\mathbf{N^p}$ are the shape function of displacement and pore pressure. Their expressions are listed as following:

$$\mathbf{\bar{u}} = \begin{bmatrix} u_1 \ v_1 \ u_2 \ v_2 \ \ldots \ u_n \ v_n \end{bmatrix}^{\mathrm{T}} \tag{7}$$

$$\mathbf{\bar{p}} = \begin{bmatrix} p_1 \ p_2 \ \ldots \ p_n \end{bmatrix}^{\mathrm{T}} \tag{8}$$

$$\mathbf{N^u} = \begin{bmatrix} N_1^u & 0 & N_2^u & 0 & \ldots & N_n^u & 0 \\ 0 & N_1^u & 0 & N_2^u & \ldots & 0 & N_n^u \end{bmatrix} \tag{9}$$

$$\mathbf{N^p} = \begin{bmatrix} N_1^p & N_2^p & \ldots & N_n^p \end{bmatrix} \tag{10}$$

Substituting Eqs. (5) and (6) into the governing equations (1) and (3), and applying the variation principle, the "$u - p$" governing equations are discretized in space as:

$$\mathbf{M\ddot{\bar{u}} + K\bar{u} - Q\bar{p}} = f^{(1)} \tag{11}$$

$$\mathbf{G\ddot{\bar{u}} + Q^{\mathrm{T}}\dot{\bar{u}} + S\dot{\bar{p}} + H\bar{p}} = f^{(2)} \tag{12}$$

$\mathbf{\bar{u}}$ and $\mathbf{\bar{p}}$ are the nodal displacements and the pore pressure vectors respectively. M, K, Q, G, S, and H are the mass, stiffness, coupling, dynamic seepage force, compressibility, and permeability matrixes respectively. $f^{(1)}$ and $f^{(2)}$ are the node force vectors. Their expressions are listed following.

$$\mathbf{M} = \int (\mathbf{N^u})^{\mathrm{T}} \rho \mathbf{N^u} d\Omega \tag{13}$$

$$\mathbf{K} = \int \mathbf{B^{\mathrm{T}} D B} \, d\Omega \tag{14}$$

$$\mathbf{Q} = \int \mathbf{B^{\mathrm{T}}} m \mathbf{N^p} d\Omega \tag{15}$$

$$\mathbf{S} = \int (\mathbf{N^p}) n \beta \mathbf{N^p} d\Omega \tag{16}$$

$$\mathbf{H} = \int (\nabla \mathbf{N^p})^{\mathrm{T}} k \nabla \mathbf{N^p} d\Omega \tag{17}$$

$$G = \int (\nabla N^{\mathbf{p}})^{\mathrm{T}} k \rho_f N^{\mathbf{u}} d\Omega \tag{18}$$

$$\nabla = \begin{bmatrix} \frac{\partial}{\partial x} \\ \frac{\partial}{\partial z} \end{bmatrix} \tag{19}$$

$$B = \begin{bmatrix} \frac{\partial}{\partial x} & 0 \\ 0 & \frac{\partial}{\partial z} \\ \frac{\partial}{\partial z} & \frac{\partial}{\partial x} \end{bmatrix} N^{\mathbf{u}}, \tag{20}$$

$$f^{(1)} = \int (N^{\mathbf{u}})^{\mathrm{T}} \rho \mathbf{g} \, d\Omega + \int (N^{\mathbf{u}})^{\mathrm{T}} \bar{\mathbf{t}} \, d\Gamma \tag{21}$$

$$f^{(2)} = -\int (N^{\mathbf{p}})^{\mathrm{T}} \nabla^{\mathrm{T}} (k\rho_f \mathbf{g}) \, d\Omega + \int (N^{\mathbf{p}})^{\mathrm{T}} \bar{\mathbf{q}} \, d\Gamma \tag{22}$$

where $m = [1, 1, 1, 0, 0, 0]^{\mathrm{T}}$, $\bar{t}$ is the stress acting on the surface of computational domain, $\bar{q}$ is the water flux on the surface of computational domain. The matrix G could be neglected in low frequency analysis proposed by Chan (1988). Under plane strain conditions, the elastic matrix D can be expressed as:

$$D = \frac{E}{(1+\nu)(1-2\nu)} \begin{bmatrix} 1-\nu & \nu & 0 \\ \nu & 1-\nu & 0 \\ 0 & 0 & \frac{1-2\nu}{2} \end{bmatrix} \tag{23}$$

where E and ν are the elastic modulus and Poisson's ratio respectively.

Temporal discretization The general procedure adopted in this study to solve the governing equations (11) and (12) at each time step, is the GNpj (Generalized Newmark pth order scheme for jth order equation) time integration scheme. This method is originally proposed by Newmark (1959), and later extended by Katona and Zienkiewicz (1985).

If the governing equations (11) and (12) are satisfied at the nth time step, then they will also be satisfied at the $(n + 1)$th time step (G is neglected):

$$M_{n+1} \ddot{\mathbf{u}}_{n+1} + K_{n+1} \bar{\mathbf{u}}_{n+1} - Q_{n+1} \bar{\mathbf{p}}_{n+1} = f_{n+1}^{(1)} \tag{24}$$

$$Q_{n+1}^{\mathrm{T}} \dot{\mathbf{u}}_{n+1} + S_{n+1} \dot{\mathbf{p}}_{n+1} + H_{n+1} \bar{\mathbf{p}}_{n+1} = f_{n+1}^{(2)} \tag{25}$$

By applying the GN22 method for the soil displacements, the acceleration, velocity and displacement at time $t_n + \Delta t$ are expressed as:

$$\ddot{\mathbf{u}}_{n+1} = \ddot{\mathbf{u}}_n + \Delta \ddot{\mathbf{u}}_n \tag{26}$$

$$\dot{\mathbf{u}}_{n+1} = \dot{\mathbf{u}}_n + \ddot{\mathbf{u}}_n \Delta t + \beta_1 \Delta \ddot{\mathbf{u}}_n \Delta t \tag{27}$$

$$\bar{\mathbf{u}}_{n+1} = \bar{\mathbf{u}}_n + \dot{\mathbf{u}}_n \Delta t + \frac{1}{2} \ddot{\mathbf{u}}_n \Delta t^2 + \frac{1}{2} \beta_2 \Delta \ddot{\mathbf{u}}_n \Delta t^2 \tag{28}$$

and applying the GN11 method for pore pressure, the the rate of pore pressure and the pore pressure are expressed as:

$$\dot{\mathbf{p}}_{n+1} = \dot{\mathbf{p}}_n + \Delta \dot{\mathbf{p}}_n \tag{29}$$

$$\bar{\mathbf{p}}_{n+1} = \bar{\mathbf{p}}_n + \dot{\mathbf{p}}_n \Delta t + \theta_1 \Delta \dot{\mathbf{p}}_n \Delta t \tag{30}$$
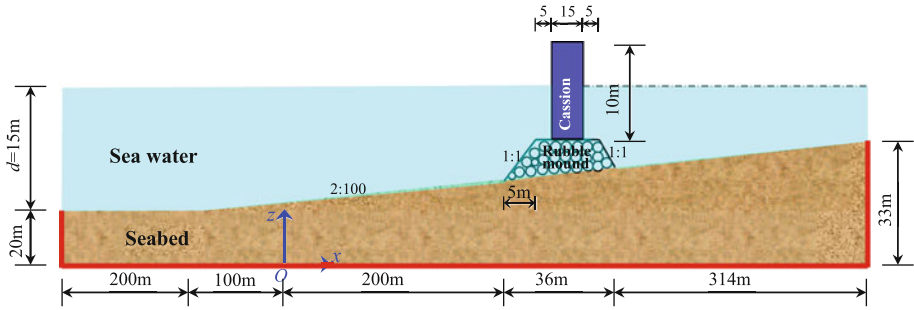
Fig. 1 The computational domain for the seabed foundation and composite breakwater

In the above schemes, if the parameters β_1, β_2 and θ satisfy following condition:

$$\beta_2 \geq \beta_1 \geq \frac{1}{2} \quad \text{and} \quad \theta_1 \geq \frac{1}{2} \tag{31}$$

then the GNpj time integration scheme is unconditionally stable (Chan 1988). In this study, the three parameters are chosen as: $\beta_2 = 0.605$, $\beta_1 = 0.6$ and $\theta_1 = 0.6$. It has been shown by Chan (1988) that the the above three values work well to evaluate the dynamic response of soil under earthquakes and ocean waves.

Substituting Eqs. (26), (27), (28), (29) and (30) into Eqs. (24) and (25), we obtain following matrix governing equation:

$$\begin{bmatrix} M_{n+1} + \frac{1}{2}K_{n+1}\beta_2\Delta t^2 & -Q_{n+1}\theta_1\Delta t \\ Q_{n+1}^T\beta_1\Delta t & S_{n+1} + H_{n+1}\beta_1\Delta t \end{bmatrix} \begin{bmatrix} \Delta\ddot{\mathbf{u}}_n \\ \Delta\dot{\mathbf{p}}_n \end{bmatrix} = \begin{bmatrix} F_{n+1}^{(1)} \\ F_{n+1}^{(2)} \end{bmatrix} \tag{32}$$

where the $F_{n+1}^{(1)}$ and $F_{n+1}^{(2)}$ are formulated as:

$$F_{n+1}^{(1)} = f_{n+1}^{(1)} + Q_{n+1}\bar{p}_n + Q_{n+1}\dot{\bar{p}}_n\Delta t - M_{n+1}\ddot{\mathbf{u}}_n - K_{n+1}\left(\bar{\mathbf{u}}_n + \dot{\bar{\mathbf{u}}}_n\Delta t + \frac{1}{2}\ddot{\bar{\mathbf{u}}}_n\Delta t^2\right) \tag{33}$$

$$F_{n+1}^{(2)} = f_{n+1}^{(2)} - S_{n+1}\dot{\bar{p}}_n - H_{n+1}(\bar{p}_n + \dot{\bar{p}}_n\Delta t) - Q_{n+1}(\dot{\bar{\mathbf{u}}}_n + \ddot{\bar{\mathbf{u}}}_n\Delta t) \tag{34}$$

In Eq. (32), the unknowns are $\Delta\ddot{\mathbf{u}}_n$ and $\Delta\dot{\mathbf{p}}_n$. At $(n+1)$th time step. they can be determined by solving Eq. (32) by taking the values determined at the n time step as the initial conditions. In this investigation, the Newton–Raphson method is adopted to solve Eq. (32). Once the incremental acceleration $\Delta\ddot{\mathbf{u}}_n$ and incremental rate of pore pressure $\Delta\dot{\mathbf{p}}_n$ are determined, the displacement of the soil and pore pressure can be accordingly obtained by applying Eqs. (28) and (30).

4 Boundary conditions

The computational domain shown in Fig. 1 is a large scale seabed-breakwater model which is as realistically as possible closed to the real cases in offshore environments. The composite breakwater is built on the sloped seabed (2:100), consisting of a rigid caisson and a rubble mound. The rubble mound is made of stone and/or gravel. The length of the top side of the rubble mound is 25 m. The slope of the two lateral sides of the rubble mound is 1:1. The dimension and coordinate of the rubble mound can be seen in Fig. 1. The horizontal length

of computational domain is 850 m. The distances from the left and right lateral side to the composite breakwater are 314 and 500 m respectively. This distance can sufficiently eliminate the effect of the lateral boundary condition on the dynamic response in the region near to the composite breakwater. In calculation, following boundary conditions are applied:

First, the bottom of seabed is considered as rigid and impermeable:

$$u = w = 0 \quad \text{and} \quad \frac{\partial p}{\partial z} = 0 \tag{35}$$

Second, the left and right lateral sides are fixed both in horizontal and vertial direction:

$$u = w = 0 \quad \text{at } x = -300 \, \text{m} \quad \text{and} \quad x = 550 \, \text{m} \tag{36}$$

Third, The hydrostatic pressure is applied on the surface of seabed and the outer surface of rubble mound breakwater. All force induced by the hydrostatic pressure is perpendicular with the surfaces (Fig. 1). The consideration of the hydrostatic pressure in seismic analysis is necessary due to that the application of the hydrostatic pressure on seabed and rubble mound breakwater could significantly change the natural frequency of seabed and rubble mound breakwater (Memos et al. 2000). It will further affect the resonance phenomenon of marine structures. In practice engineering, the large wave and earthquake is unlikely to occur simultaneously. The wave loading is not considered in this study. It is noted that the effect of vibrated seabed foundation and marine structures on the static water level is not considered in this study. The vibrated seabed and marine structures generally could lead to the generation of small wave in sea water. The experimental tests conducted by Memos et al. (2000) indicates that the dynamic pressure acting on seabed and rubble mound breakwater induced by the small wave generally accounts for a small percentage of the total pressure.

Fourth, the seismic accelerations at horizontal (E–W) and vertical (U–D) direction are applied to the two lateral sides and the bottom of computational domain simultaneously. In this study, the recorded acceleration in E–W and U–D direction are applied to the x and z direction respectively.

$$\begin{cases} (a_x)_t = (a_{\text{EW}})_t \\ \qquad\qquad\qquad\qquad \text{on lateral sides and bottom} \\ (a_z)_t = (a_{\text{UD}})_t \end{cases} \tag{37}$$

where the $(a_x)_t$ and $(a_z)_t$ are the acceleration in x and z directions on lateral sides and bottom of computational domain at time t. $(a_{\text{EW}})_t$ and $(a_{\text{UD}})_t$ are the input seismic acceleration at E–W and U–D (vertical) directions at time t. This kind of application of seismic acceleration to the boundaries of computational domain is similar with that in shaking table test and seismic centrifuge test. This method could effectively avoid the generation of reflected wave in seismic analysis. Otherwise, the viscous absorbing boundary has to be used if the seismic wave is only input at the bottom of seabed foundation in numerical simulation (Jafarian et al. 2010). In the real propagating process of seismic wave, the chosen computational domain is not enough to make the seismic wave attenuate obviously when passing through seabed foundation. Therefore, it is reasonable to apply the same seismic wave to each lateral side and the bottom of seabed foundation at each analysis time step (Chan 1988; Ou 2009).

5 Earthquake input data

In this study, the acceleration wave induced by the Japan 311 off the pacific coast of Tohoku earthquake ($M_L = 9.0$) is used as the earthquake loading to apply the dynamic loading to the
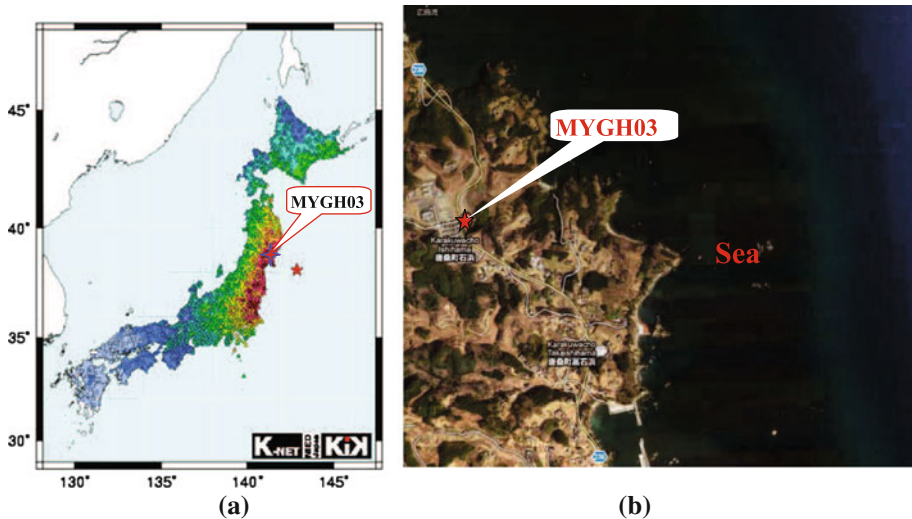
Fig. 2 The position of the observation station MYGH03 (installed by NIED in Japan). It locates at the point (141.6412E, 38.9178N) near to the east coast of Japan

seabed foundation. In order to apply a strong seismic loading to the seabed foundation, the seismic wave of accelerations recorded at a place where near to the epicenter of earthquake, and located near to the coastal line is chosen as the input seismic accelerations in calculation.

The seismic acceleration wave recorded at the observation station labeled as MYGH03 (located at 141.6412E, 38.9178N) is chosen as the input earthquake loading (provided by National Research Institute for Earth Science and Disaster Prevention (NIED) in Japan). The distance from this chosen observation station to the epicenter (142.9E, 38N) is 154 km (Fig. 2a); and this observation station is near to the coastal line of pacific ocean (Fig. 2b). There-fore, the chosen input seismic acceleration wave in this study is similar as close as possible with the real seismic wave propagating to seabed foundation.

There are two kinds of seismic waves recorded at observation station MYGH03. One is recorded on ground, another is recorded at the position underground. In this study, the seismic acceleration wave recorded underground is used (Fig. 3) due to that it is not affected by the site conditions. From Fig. 3, it is found that the seismogenic fault in the subduction zone of pacific plate dislocates two times in the earthquake. The vibration induced by he first dislocation is more strong than that induced by the second dislocation. The maximum acceleration in E–W and U–D (vertical) direction is 1.33 and 1.21 m/s^2 respectively. The duration of this strong earthquake is about 200 s (from 25 to 225 s).

6 Results and discussion

6.1 Consolidation of seabed under composite breakwater

In the offshore environment, the seabed generally has experienced the consolidation process under the seawater loading and self-gravity in the geological history. Additionally, after the composite breakwater is constructed on the seabed, the seabed beneath and near to the com-posite breakwater will be compressed, and deform under the weight of composite breakwater.
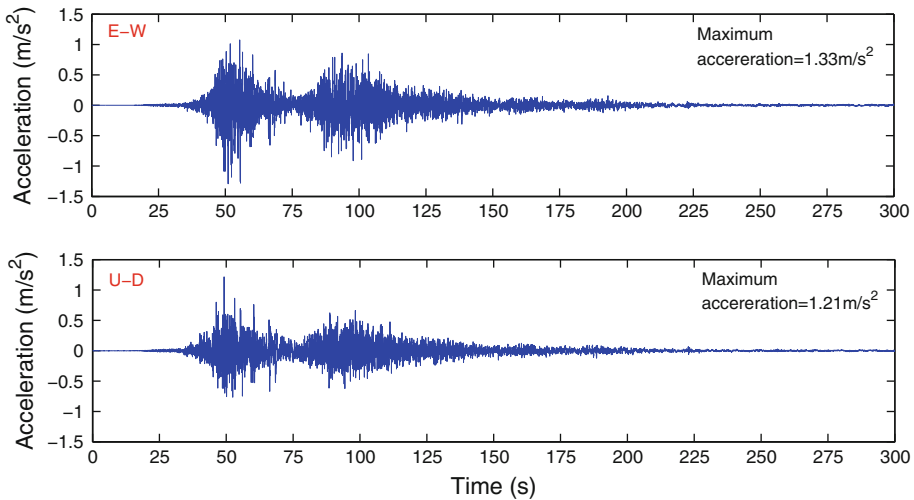
Fig. 3 The input seismic acceleration wave recorded at observation station MYGH03 in the Japan 311 off the pacific coast of Tohoku earthquake ($M_L = 9.0$)

Table 1 Properties of seabed foundation and composite breakwater used in numerical computation

Medium	G (N/m^2)	ν	k (m/s)	n	d_{50} (mm)	Sr
Seabed	6.0×10^7	0.333	1.0×10^{-5}	0.25	0.2	0.98
Rubble mound	1.0×10^8	0.333	2.0×10^{-1}	0.35	500	0.99
Caisson	5.0×10^{10}	0.25	0.0	0.0	–	0.0

Finally, the seabed will reach a new balanced state based on the previous consolidation status under hydrostatic sea water pressure and composite breakwater loading. From the point of view of physics, in order to simulate the seismic response of seabed and marine structures, the initial consolidation state of seabed under hydrostatic pressure and weight of composite breakwater should be firstly determined. Then, this consolidation status is taken as the initial condition for seismic analysis. The properties of seabed foundation and composite breakwater used in consolidation and seismic response analysis are listed in Table 1.

Figure 4 illustrates the distributions of effective stresses, shear stress and the pore pressure in porous seabed under hydrostatic pressure and the weight of composite breakwater after the seabed foundation consolidating adequately. Figure 5 shows the distributions of horizontal and vertical displacements in seabed foundation. It can be seen from Fig. 4 that the contours of pore pressure in seabed foundation are basically layered, which is consistent with the distribution of hydrostatic water pressure. The magnitudes of effective stresses in the seabed foundation under composite breakwater increase significantly comparing with that when there is no marine structures. Additionally, there are two zones in seabed near to the two roots of rubble mound where the shear stress concentrates. It is possible for this concentrated shear stress to make the seabed foundation fail (known as shear failure) in engineering. Figure 5 indicates that the composite breakwater subsides about 30 mm induced by its weight; and the seabed foundation is compressed, and the soil particles move toward two sides. Due to that the composite breakwater is built on a coastal slope, the horizontal displacement at the two
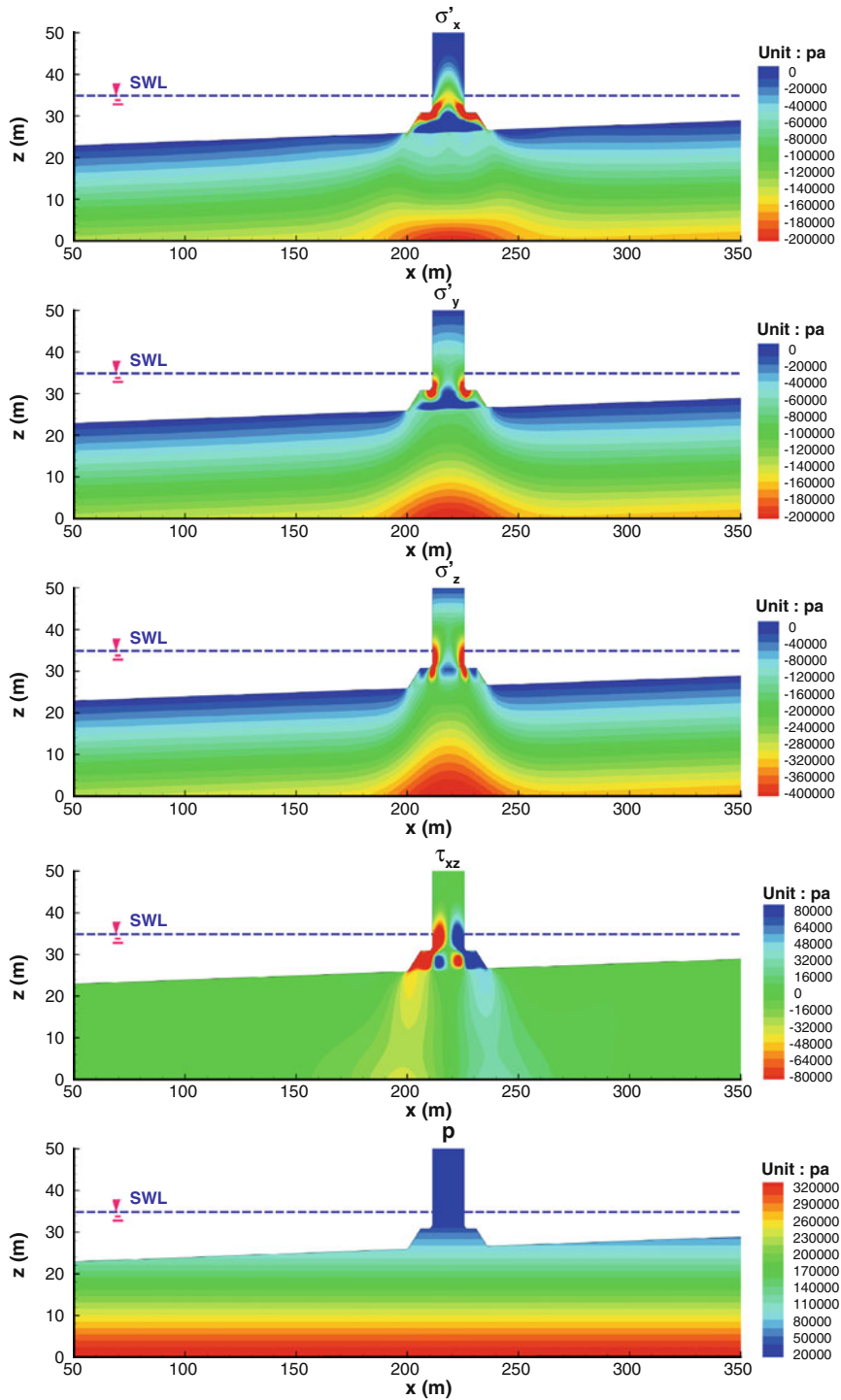
Fig. 4 The distribution of pore pressure, effective stresses in seabed foundation and composite breakwater in the consolidation status
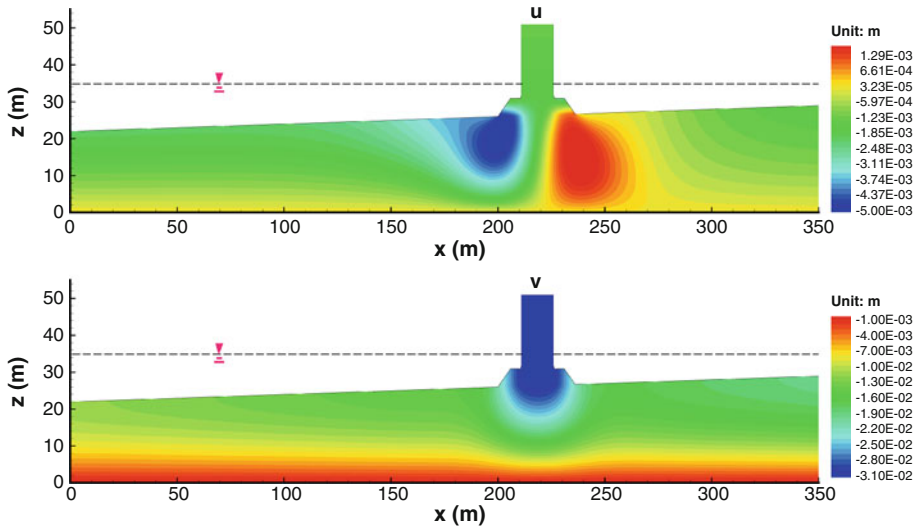
Fig. 5 The distribution of displacements in in seabed foundation and composite breakwater in the consolidation status
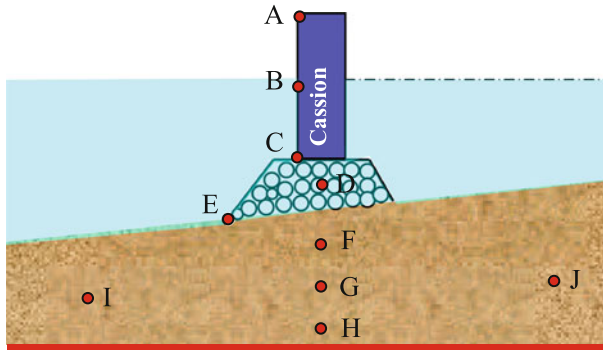

Fig. 6 The position of points in seabed foundation and on composite breakwater for dynamical monitoring in numerical modelling

sides of composite breakwater is not symmetric. The horizontal displacement at left side of composite breakwater is obviously greater than that at the right side.

6.2 Seismic response composite breakwater

Taking the consolidation status of seabed foundation under hydrostatic pressure, self-gravity and compression of composite breakwater determined above as the initial condition, the seismic response of composite breakwater and its seabed foundation under a strong seismic wave loading is investigated using the FEM model.

It is impossible to analyze the seismic response of all points in composite breakwater and seabed foundation. In this study, some typical points on the composite breakwater and in seabed foundation are chosen to illustrate the seismic response of composite breakwater and its seabed foundation (see Fig. 6). The coordinates of these points are listed in Table 2.

Table 2 The coordinates of typical points on composite breakwater and seabed foundation used in analysis (unit: m)

Point	Coordinate		Point	Coordinate	
	x	z		x	z
A	211	51	F	218.5	23.94
B	211	46	G	218.5	13.8
C	211	31	H	218.5	4.87
D	218.5	28.5	I	140	12.97
E	200	26	J	300.7	13.9

Figure 7 shows the horizontal and vertical acceleration response of composite breakwater at point A, B and C under the strong seismic loading. It can be seen from Fig. 7 that the horizontal seismic response is much more intensive than that in vertical direction. This could attribute to that the gravity of seabed foundation and composite breakwater can effectively suppress the seismic response in vertical direction. The vertical seismic response at point A, B and C are basically the same; the maximum vertical seismic response acceleration is about 2.36–2.39 m/s^2. However, it is significantly different in the horizontal direction. The amplification of horizontal seismic response is obvious from the bottom to the top of caisson. The maximum horizontal seismic response acceleration increase about 2.4 m/s^2 if the height of points increasing 10 m in the caisson. This results suggest that the ratio of height and width of caisson built on rubble mound must be limited in engineering.

Figure 8 illustrates the horizontal and vertical seismic response velocity and displacement of composite breakwater at point A. From Fig. 8, it also can be seen that the horizontal seismic response is much more intensive than the vertical seismic response. The maximum response velocity and displacement reach up 2.29 m/s and 46 cm, while they are only 0.34 m/s and 7.3 cm in the vertical direction. The horizontal seismic response is about 7 times of the vertical seismic response at point A.

The point A, B and C are all on the caisson. Following, the seismic responses of point D and E which are in/on rubble mound are demonstrated. Figure 9 shows the acceleration seismic response at point D and E. Due to the fact that the ratio between the height and the width of rubble mound is very small, and these two points are closed, the difference of seismic response at these two points is insignificant. The acceleration seismic responses at point D and E are also very similar with that at point C. The maximum acceleration is about 7.5–8.0 m/s^2 at horizontal direction, 2.0–2.4 m/s^2 at vertical direction.

In the rubble mound, the void is filled with pore water. The earthquake makes the pore water pressure variates correspondingly. Figure 10 shows the earthquake induced pore pressure at point D in the rubble mound. As illustrated in Fig. 10, before $t = 25$ s (seismic wave doesn't arrive the site), the pore pressure is equal to the hydrostatic pressure. Once the seismic wave arrives the site, the pore pressure in rubble mound begins to vibrate; and the amplitude of variation is positively related to the input seismic wave. The maximum seismic induced pore pressure is 5832 pa.

The seismic acceleration response spectrum of composite breakwater to the input seismic wave is an important basis in the anti-seismic design. The fortification acceleration could be determined from the seismic acceleration response spectrum based on the natural frequency of composite breakwater. Figure 11 illustrates the seismic acceleration response spectrum of composite breakwater to the input seismic wave at point A and E. From Fig. 11, it can be seen that the horizontal (E–W) response of composite breakwater is much more intensive than the vertical (U–D) response. Comparing with the response spectrum of input seismic wave, the
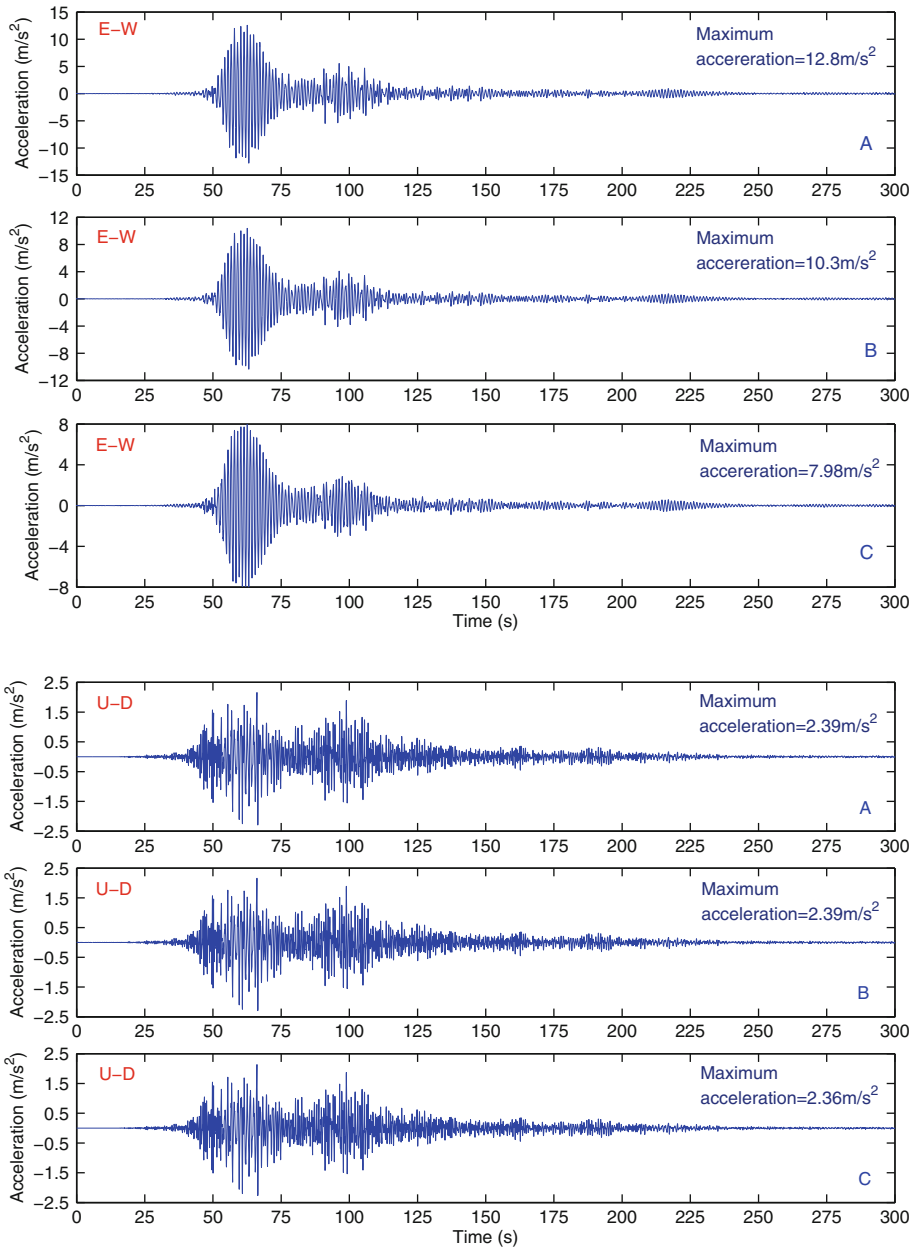
Fig. 7 Horizontal (E–W) and vertical (U–D) acceleration response of composite breakwater at point A, B and C under seismic loading

horizontal response of composite breakwater is amplified significantly for all periods; while this amplification only exists in the range of 0.3–2.0 s for the vertical response of composite breakwater. When natural period of composite breakwater is around 1.2 s, the resonance of composite breakwater to the input seismic wave occurs. This resonance should be avoid in
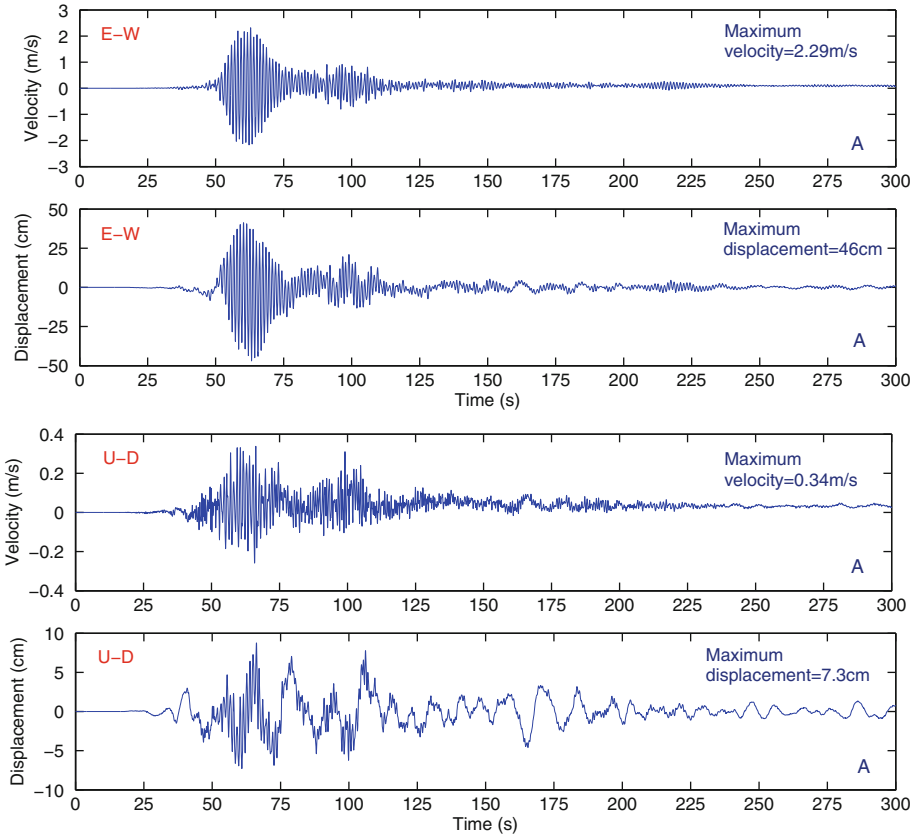
Fig. 8 The horizontal and vertical seismic response velocity and displacement of composite breakwater at point A
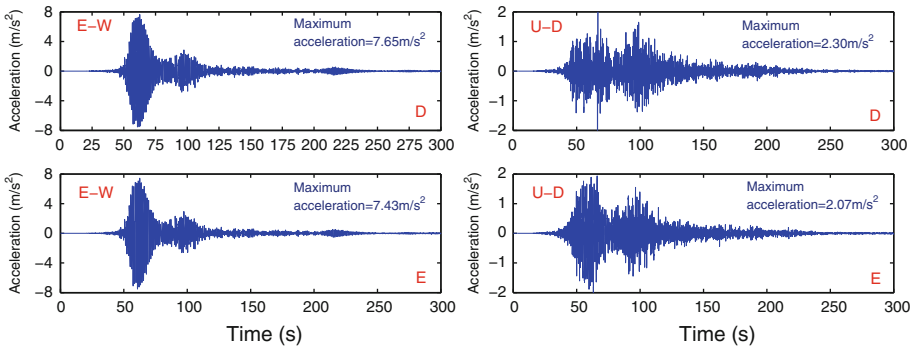
Fig. 9 Horizontal and vertical acceleration response of composite breakwater at point D and E under seismic loading
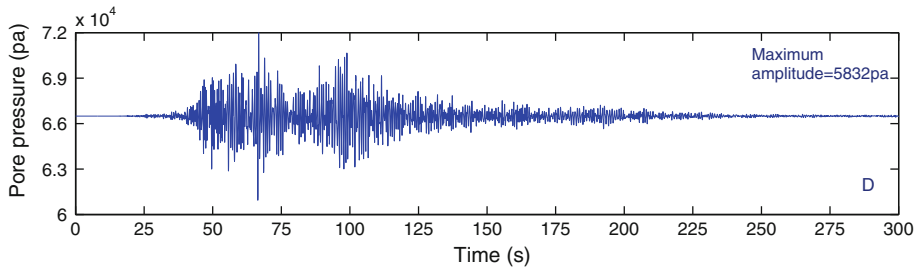
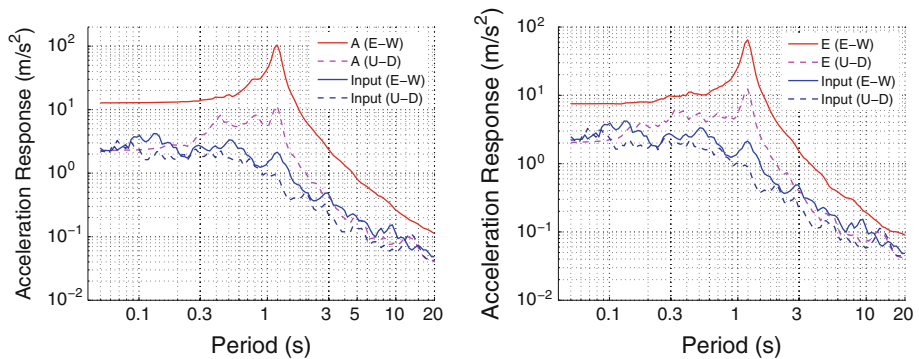**Fig. 10** Seismic induced pore pressure response in rubble mound at point D

Fig. 11 Seismic acceleration response spectrum of composite breakwater to the input seismic wave at point A and E (damping ratio = 5 %)

structure design. The best way is to control the natural period of composite breakwater is less than 0.3 s.

6.3 Seismic response of seabed foundation

The seabed is natural foundation for the marine structures constructed in offshore area. The seismic response of seabed foundation is a very important factor for evaluation of the stability in earthquake events. In this part, the seismic response of seabed foundation under strong earthquake is investigated.

Figure 12 shows the horizontal and vertical seismic acceleration response at point F, G and H in seabed foundation under the composite breakwater. From Fig. 12, it can be found that: (1) Horizontal seismic response is more intensive than the vertical seismic response. (2) The horizontal seismic response is amplified from bottom to surface of seabed foundation. (3) The vertical seismic response is also amplified from bottom to surface of seabed foundation; this is different with that in composite breakwater. Therefore, the input seismic wave is amplified by the porous seabed foundation both in horizontal and vertical direction. The ratio between the maximum horizontal and vertical acceleration at one point in seabed foundation is positively with the distance to the bottom of seabed foundation. For example, the ratio at point F, G and H is 1.94, 2.84 and 3.19 respectively.

Similar with the pore pressure variation at point D in rubble mound, the seismic wave also leads to the variation of pore pressure at point F, G and H in seabed foundation. Figure 13 illustrates the seismic response of pore pressure in seabed foundation. Before seismic wave
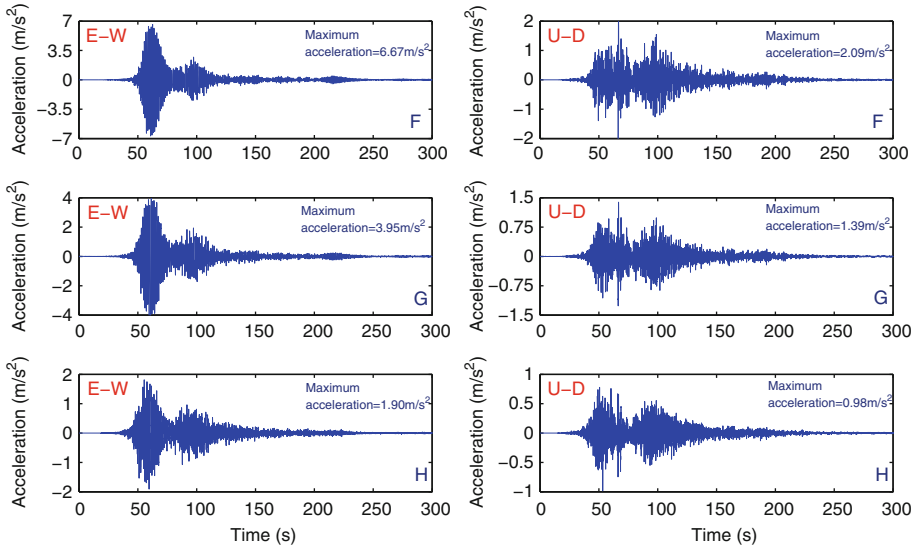
Fig. 12 The horizontal and vertical seismic acceleration response in seabed foundation at point F, G and H
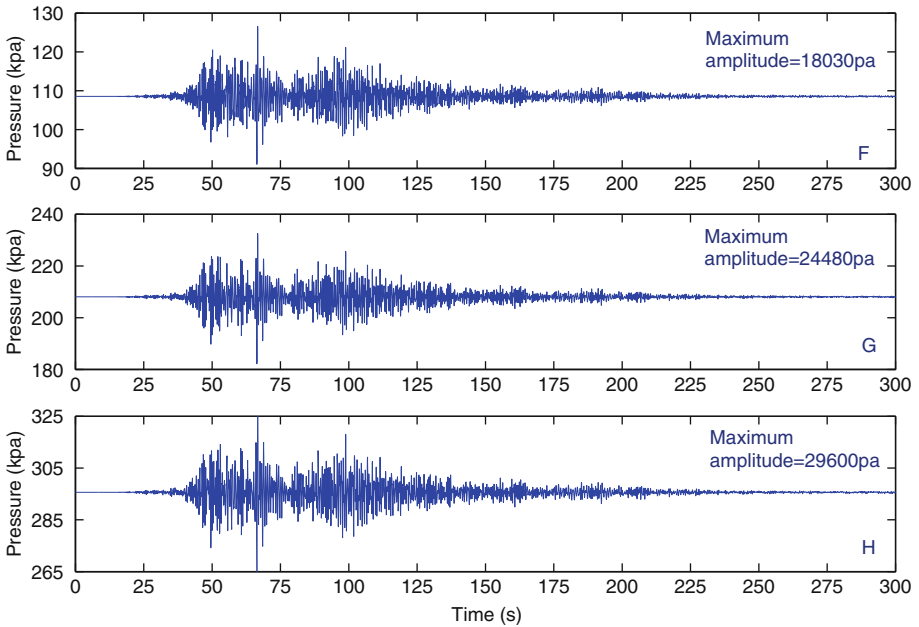

Fig. 13 The earthquake induced pore pressure response in seabed at F, G and H

arriving (t = 25 s), the pore pressure keeps as the hydrostatic pressure. The pore pressure begins to vibrate after seismic wave arriving the site. A important phenomenon observed from Fig. 13 is that the earthquake induced pore pressure in seabed is positively with the buried depth. The maximum earthquake induced pore pressure is 18.03, 24.48 and 29.60 kPa at point F, G and H respectively.
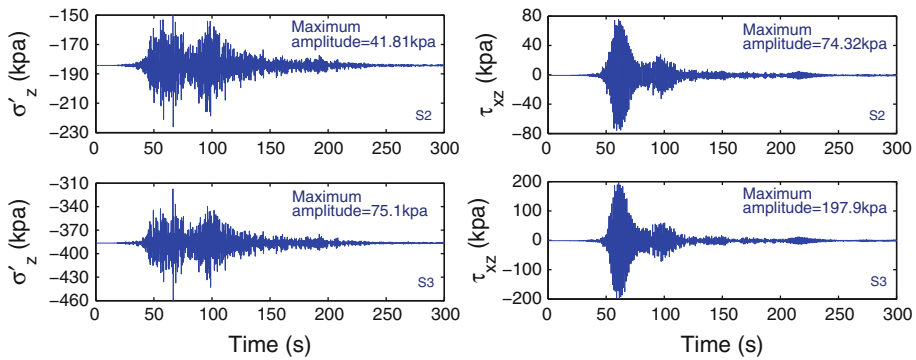
Fig. 14 The seismic wave induced stress response in seabed foundation at S2 (218.5 m, 25.0 m) and S3 (218.5 m, 6.1 m) under the composite breakwater

According to the effective stresses principle, the variation of pore pressure in seabed foundation will results in the variation of effective stresses. Figure 14 illustrates the earthquake induced response of vertical effective stress σ'_z and shear stress τ_{xz} at point S2 (218.5 m, 25.0 m) and S3 (218.5 m, 6.1 m), which are under the composite breakwater. In evaluation of the stability of marine structures, the vertical effective stress σ'_z and shear stress τ_{xz} are directly related to the liquefaction and the shear failure. As illustrated in Fig. 14, the effective stresses in seabed foundation also vibrate corresponding to the seismic wave propagating to the site. The maximum variation amplitude of effective stress is also positively related to the buried depth. Due to the fact that the S2 and S3 are located at the approximate symmetrical line $x = 218.5$ m, the initial shear stress τ_{xz} before $t = 25$ s is near to 0.

All the points analyzed above are under the composite breakwater. Following, the seismic response at two typical points I and J located at the left and right hand side of composite breakwater is investigated (the height of I and J nearly is same with point G). Figure 15 demonstrates the horizontal and vertical seismic response of acceleration at point I and J. Comparing with the seismic response of acceleration at point G, it is found that the horizontal acceleration response at point J is very similar with that at point G; while the horizontal acceleration response at point I is significantly different with that at point G and J. The maximum acceleration is only 2.79 m/s^2 at point I. It is 3.95 and 3.83 m/s^2 respectively at point G and J. A obvious phenomenon observed from the vertical acceleration response at point I, G and J is that vertical maximum acceleration response in seabed foundation is negatively related to the overburdened weight of soil and composite breakwater. The response acceleration of points under the composite breakwater is smallest due to the compression of composite breakwater; and the response acceleration of points located at the left hand side of composite breakwater is greater than that in the right hand side of composite breakwater.

Figures 16 and 17 show the seismic wave induced pore pressure and effective stress response at point I and J. Comparing with the seismic response of pore pressure at point G, it is found that the seismic wave induced pore pressure in seabed under the composite breakwater is smallest, for example, the seismic wave induced pore pressur at point G is only 24.48 kPa; while, it is 32.79 and 35.85 kPa respectively at point I and J.

Figure 18 illustrates the seismic acceleration response spectrum of seabed foundation to the input seismic wave at point F and H. From Fig. 18, it is found that the horizontal and vertical response basically are not amplified at point H, located at the position near to the bottom of seabed foundation; while, horizontal response has been greatly amplified greatly at point
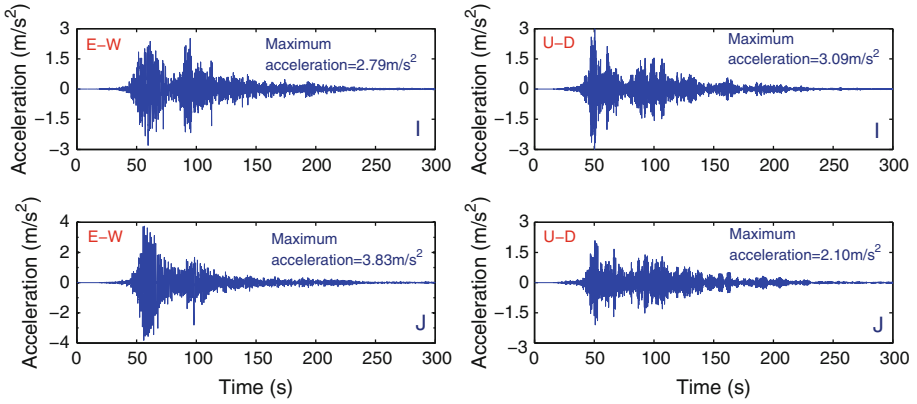
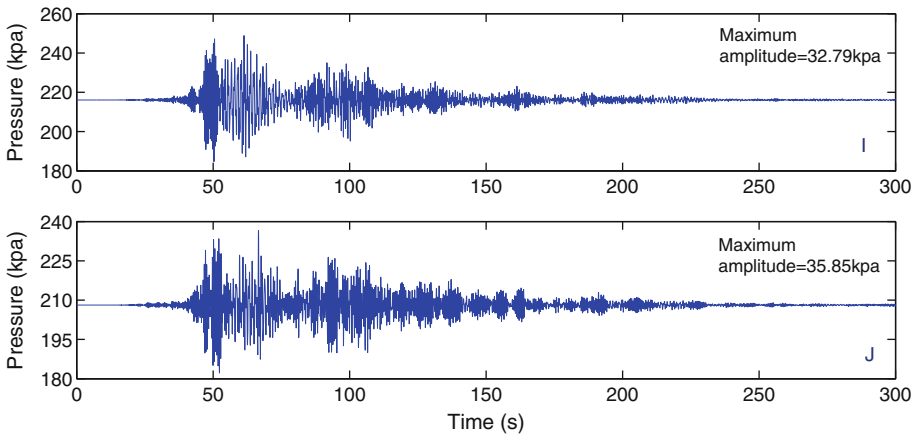**Fig. 15** The seismic acceleration response in seabed foundation at point I and J

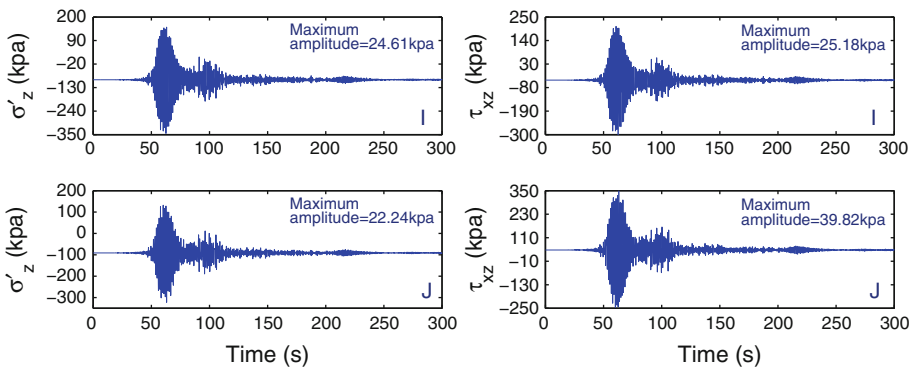**Fig. 16** The seismic wave induced pore pressure response in seabed at point I and J

Fig. 17 The seismic wave induced stress response in seabed foundation at point I and J
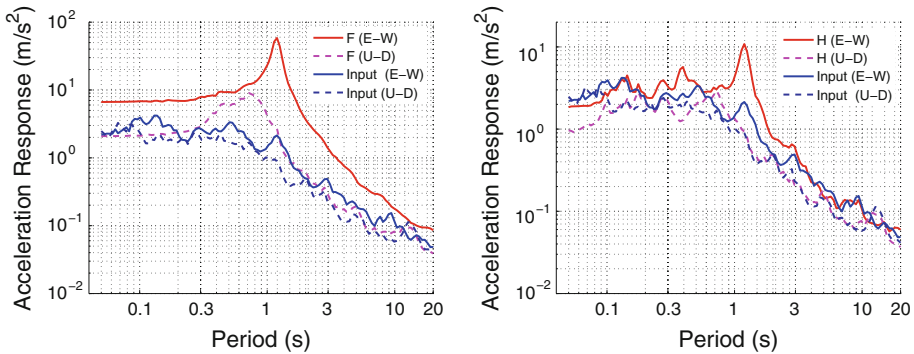
Fig. 18 Seismic acceleration response spectrum of seabed foundation to the input seismic wave at point F and H (damping ratio = 5 %)

F, located at the position near to the surface of seabed foundation. The vertical response could also be amplified if the natural period of seabed foundation is in the range of 0.3–1.2 s. The resonance period in the seabed foundation is also 1.2 s. It is indicated that the amplification of seismic response in sea foundation is negatively related to the buried depth of points.

6.4 Transient liquefaction prediction in seabed foundation

The liquefaction in seabed foundation of marine structures under dynamic loading, such as ocean wave and earthquake, has been recognized by geotechnical engineers as a main reason for the failure and instability of structures built on seabed in engineering. The liquefaction induced failure of marine structure by the shaking of soil has been well documented in previous literatures (Wyllie 1986; Memos and Protonotarios 1993; Iai and Kameoka 1993; Sugano et al. 1999; Sumer et al. 2002; Katopodi and Iosifidou 2004; Yuksel et al. 2004). More detail review about the earthquake-induced liquefaction around marine structures can be found in Sumer et al. (2007). The liquefaction analysis is necessary if the seabed foundation is consist of liquefiable soil in engineering. In this part, the transient liquefaction in poro-elastic seabed foundation under a composite breakwater excited by the strong earthquake loading is investigated by adopting the 1D and 3D liquefaction criterion proposed by Okusa (1985) and Tsai and Lee (1995) based on the effective stresses.

The 1D liquefaction criterion proposed by Okusa (1985) is:

$$- (\gamma_s - \gamma_w)(h - z) \le \sigma'_{zd} \quad \text{or } \sigma'_z \ge 0 \tag{38}$$

where the γ_s and γ_w are the unit weight of soil and pore water. h is the thickness of seabed, z is the vertical coordinate of point. σ'_{zd} is the dynamic vertical effective stress induced by the earthquake loading. σ'_z is the vertical effective stress, which is the sum of initial vertical effective stress and dynamic vertical effective stress σ'_{zd}. Equation (38) means the soil will liquefy if the dynamic vertical effective stress could overcome the prevention of initial weight of soil provided by overlying soil layers; or there is no vertical contact stress (compressive stress) between the soil particles.

Under the same frame of Okusa (1985), Tsai and Lee (1995) further extended the 1D criterion to 3D situation:

$$- \frac{1 + 2K_0}{3}(\gamma_s - \gamma_w)(h - z) \le \sigma'_{zd} \quad \text{or } (\sigma'_x + \sigma'_y + \sigma'_z) \ge 0 \tag{39}$$
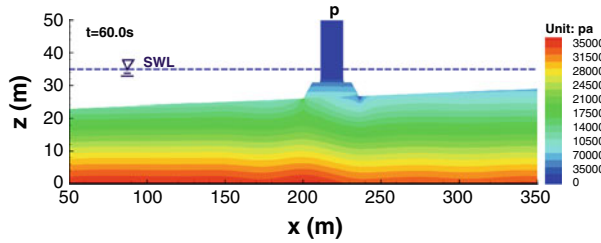
Fig. 19 The distribution of pore pressure (hydrostatic plus seismic wave induced pressure) in seabed foundation at time $t = 60$ s
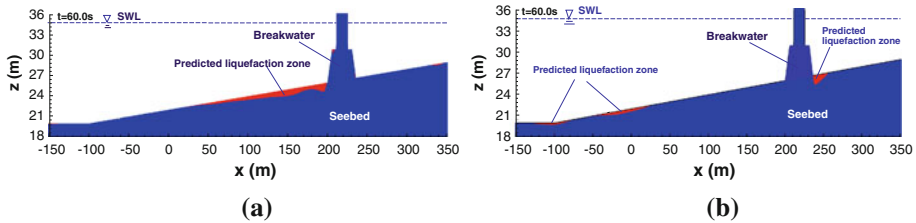

Fig. 20 The Earthquake induced liquefaction zone in seabed foundation at time $t = 60$ s. **a** 1D liquefaction criterion, **b** 3D liquefaction criterion

where the K_0 is the lateral compressive coefficient of soil. The σ'_x and σ'_y are the horizontal effective stresses in x and y direction. Obviously, the effect of horizontal effective stress on the liquefaction of soil is considered. However, this 3D liquefaction criterion is just based on the idea of average. The physical effect of σ'_x and σ'_y on liquefaction is not clear.

As analyzed in above parts, the pore pressure in seabed foundation vibrates corresponding to the excitation of seismic wave. This seismic wave induced dynamic pore pressure in seabed foundation is the main reason for the seabed liquefaction. Figure 19 is the distribution of pore pressure in seabed foundation at time $t = 60$ s. All demonstrated in Fig. 19, the seismic induced dynamic pore pressure in the lower part of seabed foundation is significant. This phenomenon is consistent with the conclusion made in above part that the seismic wave induced dynamic pore pressure is positively related to the buried depth in seabed foundation. Although the seismic wave induced dynamic pore pressure in upper part of seabed is less than that in lower part of seabed, the seismic wave induced transient liquefaction still occurs in the upper part of seabed due to the fact that the overburdened weight of soil and composite breakwater is relatively small in upper part of seabed. Figure 20 shows the earthquake induced liquefaction zone in seabed foundation at a typical time $t = 60$ s predicted by 1D and 3D liquefaction criterion.

From Fig. 20, it can be seen that there are liquefaction zones in regions near to the seabed surface under seismic wave loading. However, the range and the position of liquefaction zones predicted by 1D and 3D criterion is significantly different. At present, there is no any experimental data to demonstrate which criterion is better. Therefore, the liquefaction zones predicted by the two criterion are both shown. Which liquefaction criterion (1D or 3D) could be more accurate to predict the liquefaction in sandy soil needs to be studied in the future.

Figure 21 illustrates the predicted liquefaction depth in seabed foundation at $x = 180.8$ m under the strong earthquake loading. As illustrated in Fig. 21, the liquefaction depth in seabed foundation is positively related to the acceleration of input seismic wave. The maximum liquefaction depth predicted by 3D criterion is much greater than that predicted by 1D criterion. The maximum liquefaction depth at $x = 180.7$ m predicted by 3D and 1D criterion is 5.2 and
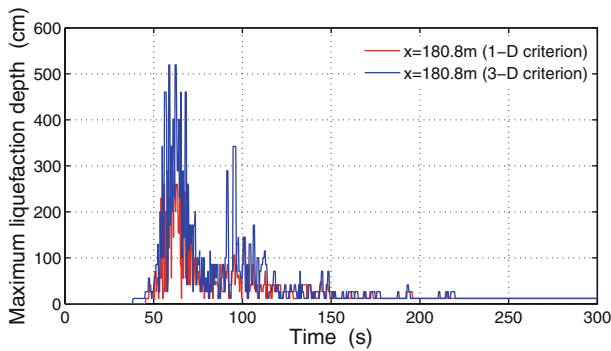
Fig. 21 The predicted liquefaction depth in seabed foundation at $x = 180.8$ m using 1D and 3D liquefaction criterion
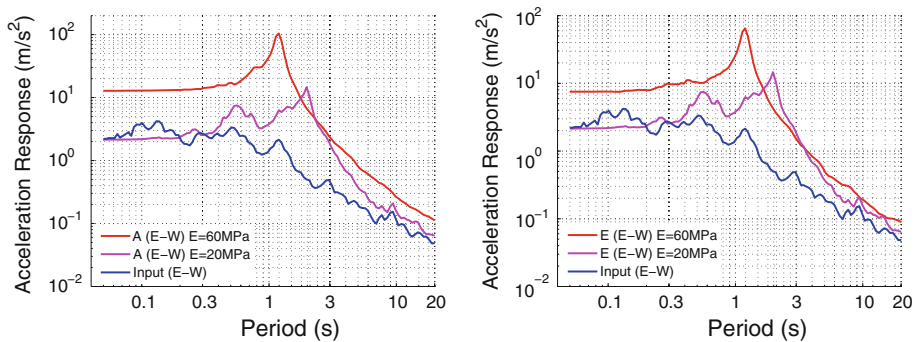

Fig. 22 Horizontal (E–W) seismic acceleration response spectrum (damping ratio $= 5\%$) at point A and E on composite breakwater built on seabed foundation with different Young's modulus (E)

2.6 m respectively. This maximum earthquake induced liquefaction depth should be taken into consideration in design of marine structures built in offshore area.

6.5 Effect of seabed properties on the seismic response of composite breakwater

In engineering application, the porous seabed chosen as the foundation of marine structures is different from cases to cases. It results in the property parameters of seabed foundation are various. How the seabed properties affect the seismic response of composite breakwater is a problem for coastal engineers. As analyzed in above parts, we know that the horizontal seismic response of composite breakwater is much intensive than the vertical seismic response to the input seismic wave. Here, the horizontal (E–W) seismic responses on point A (top of caisson) and E (lower right corner of rubble mound) are taken as the representative to investigate the effect of seabed properties on the seismic response of composite breakwater.

Figure 22 illustrates the horizontal seismic acceleration response spectrum at point A and E on the composite breakwater built on the seabed foundation with different Young's modulus (E). From Fig. 22, it is found that Young's modulus (E) of the seabed foundation has very significant effect on the seismic response of composite breakwater. The seabed foundation with $E = 20$ MPa (referred as soft seabed foundation) can effectively absorb the seismic wave energy, and decrease the seismic response of composite breakwater. In engineering
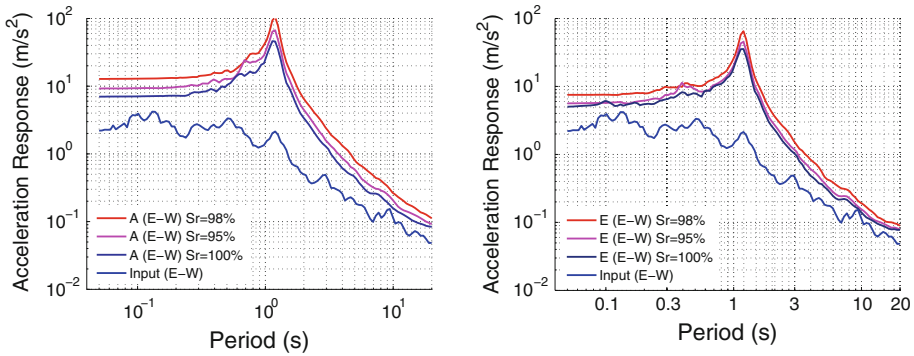
Fig. 23 Horizontal (E–W) seismic acceleration response spectrum (damping ratio = 5 %) at point A and E on composite breakwater built on seabed foundation with different saturation (Sr)
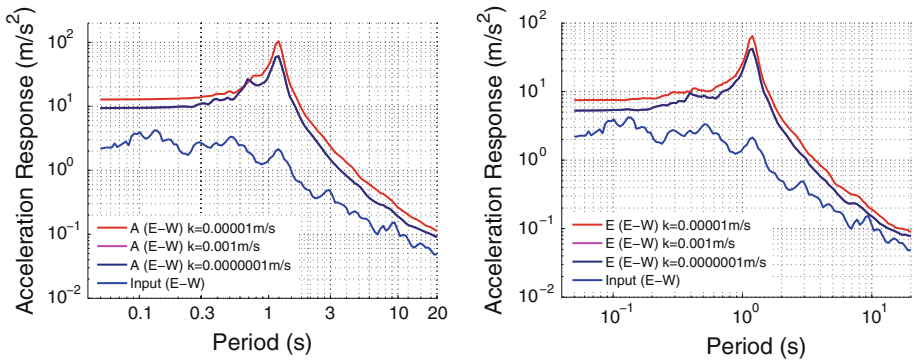
Fig. 24 Horizontal (E–W) seismic acceleration response spectrum (damping ratio = 5 %) at point A and E on composite breakwater built on seabed foundation with different permeability (k)

practice, the bearing capacity maybe is a problem for soft seabed foundation. If the requirement of bearing capacity is satisfied by soft bed, it seems that the soft seabed foundation is more beneficial for marine structures to keep their stability in strong earthquake events. From Fig. 22, it can be seen that the soft seabed foundation could make the resonance period of composite breakwater move backward, for example, the resonance period is 2.0 s for seabed foundation with $E = 20$ MPa; while it is 1.2 s for seabed foundation with $E = 60$ MPa. The soft seabed foundation only could amplify the seismic response in the period range of 0.3–7.0 s; while, the hard seabed foundation amplify all the seismic response for all frequency components. For the same frequency component, the amplification in soft seabed is much less than that in hard seabed.

Figure 23 illustrates the horizontal seismic acceleration response spectrum at point A and E on the composite breakwater built on the seabed foundation with different saturation Sr. From Fig. 23, it is found that the effect of saturation of seabed foundation is not as significant as the Young's modulus. The amplification for the seismic wave in fully saturated seabed is smallest; while, the amplification is greatest in seabed foundation with $Sr = 98$ %. Therefore, the fully seabed foundation is beneficial for the stability of composite breakwater. The variation of saturation of seabed couldn't change the resonance frequency of composite breakwater.

Figure 24 illustrates the horizontal seismic acceleration response spectrum at point A and E on composite breakwater built on seabed foundation with different permeability k. It is also can be seen that the effect of permeability of seabed foundation is not as significant as the young's modulus. The seabed foundation with large permeability (1.0×10^{-3} m/s) or very small permeability (1.0×10^{-7} m/s) could decreases the seismic response of composite breakwater comparing with the seabed with medium permeability (1.0×10^{-4}–1.0×10^{-5} m/s). The variation of permeability of seabed foundation also couldn't change the resonance response of composite breakwater.

7 Conclusions

In this study, adopting the Biot's dynamic equation "$u - p$" approximation proposed by Zienkiewicz et al. (1980) as the governing equation, the seismic response of a composite breakwater and its seabed foundation to the Japan 311 off pacific coast of Tohoku earthquake is investigated using FEM numerical model. Based on the the numerical results, following conclusions are made:

(1) It is necessary to take the consolidation status of seabed foundation under hydrostatic pressure, self-gravity and compression of composite breakwater as the initial condition for the seismic response analysis. The assumption of all initial values of displacements, effective stresses and pore pressure are zero is inappropriate.

(2) The seismic response of composite breakwater is very strong to the input seismic wave. The horizontal response is much intensive than the vertical response. The maximum response acceleration in horizontal (E–W) and vertical (U–D) direction is 12.8 and 2.39 m/s^2 at the top of composite breakwater. The composite breakwater sway strongly under the earthquake loading. The maximum horizontal and vertical displacement reach up 46 and 7.3 cm respectively at the top of composite breakwater.

(3) The amplification of seismic wave is significant in caisson. The seismic response at the top of composite breakwater is most strong. While, this amplification is insignificant in rubble mound due to that its slenderness ratio is small.

(4) The amplification of seismic wave is also significant in seabed foundation both in horizontal and vertical direction; and this amplification is positively related to the buried depth of points. The seismic response of upper seabed is more strong than that in lower seabed.

(5) Under the excitation of input seismic wave, the pore pressure in rubble mound and seabed foundation vibrates. The amplitude of dynamic variation is also positively related to the buried depth of points. Correspondingly, the effective stresses in rubble mound and seabed foundation also vibrate.

(6) From the seismic acceleration response spectrum of composite breakwater and upper seabed foundation, it is found that the horizontal seismic wave is amplified for all frequency components; while the vertical seismic wave is amplified only for the frequency components of 0.8–3.3 Hz.

(7) The transient liquefaction of seabed could occur if the zones near to the seabed surface under the earthquake loading. For the seabed foundation with properties lised in Table 1 under the input seismic wave loading, the maximum liquefaction depth is 2.6 m (1D criterion) and 5.2 m (3D criterion) respectively. In anti-seismic design, the maximum liquefaction depth should be taken into consideration.

(8) The parametric study indicates that the young's modulus *E* of seabed foundation could significantly affect the seismic response of composite breakwater. The soft seabed foundation could effectively absorb the seismic wave energy, and decrease the seismic response of composite breakwater to the input seismic wave. But it must be guarantee that the soft seabed foundation has sufficient bearing capacity to support the composite breakwater steadily in engineering practice.

References

Arablouei A, Gharabaghi ARM, Ghalandarzadeh A, Abedi K, Ishibashi I (2011) Effects of seawater-structure-soil interaction on seismic performance of caisson-type quay wall. Comput Struct 89(23–24):2439–2459

Byme P (1991) A cyclic shear-volume coupling and pore-pressure model for sand. In: Proceedings of 2nd international conference on recent advances in geotechnical earthquake engineering and soil dynamics, vol 1.24, pp 47–55

Chan AHC (1988) A unified finite element solution to static and dynamic problems of geomechanics. PhD thesis, University of Wales, Swansea Wales

Chen B-F (2000) Dynamic responses of coastal structures during earthquakes including sedimentseastructure interaction. Soil Dyn Earthq Eng 20(5–8):445–467

Chen B-F, Huang C-F (2002) Hydrodynamic forces on concrete sea wall and breakwater during earthquakes: effects of bottom sediment layers and back-fill soil. Ocean Eng 29(7):783–814

Cihan K, Yuksel Y (2011) Deformation of rubble-mound breakwaters under cyclic loads. Coast Eng 58(6):528–539

Iai S, Kameoka T (1993) Finite element analysis of earthquakeinduced damage to anchored sheet pile quay walls. Soils Found 33(1):71–91

Jafarian Y, Alielahi H, Abdollahi AS, Vakili B (2010) Seismic numerical simulation of breakwater on a liquefiable layer: IRAN LNG port. Electron J Geotech Eng 15 D:1–11

Katona MG, Zienkiewicz OC (1985) A unified set of single step algorithms. Part 3: the beta-m method, a generalisation of the Newmark scheme. Int J Numer Methods Eng 21:1345–1359

Katopodi I, Iosifidou K (2004) Impact of the lefkada earthquake 14-08-2003 on marine works and coastal regions. In: Proceedings of 7th panhellenic geographical conference, Mytilene, Greece, pp 363–370

Kiara A, Memos C, Tsiachris A (2004) Some practical aspects on the seismic behavior of rubble-mound breakwaters. In: Ports 2001: America's ports—gateways to the global economy—proceedings of the ports 2001 conference, vol 108, pp 1–10

Memos C, Bouckovalas G, Tsiachris A (2000) Stability of rubble-mound breakwaters under seismic action. In: Coastal engineering 2000—proceedings of the 27th international conference on coastal engineering, ICCE 2000, vol 276, pp 1585–1598

Memos C, Protonotarios JN (1993) Patras breakwater failure due to seismic loading. In: Proceedings of the coastal engineering conference, vol 3, pp 3343–3356

Memos CD, Kiara A, Pavlidis E (2003) Coupled seismic response analysis of rubble-mound breakwaters. Proc Inst Civ Eng Water Marit Eng 156(1):23–31

Mohajeri M, Ichii K, Tamura T (2004) Experimental study on sliding block concept for caisson walls. J Waterw Port Coast Ocean Eng 130(3):134–142

Newmark NM (1959) A method of computation for structural dynamics. J Eng Mech Div ASCE 85:67–94

Okusa S (1985) Wave-induced stress in unsaturated submarine sediments. Geotechnique 35(4):517–532

Ou J (2009) *Three-dimensional numerical modelling of interaction between soil and pore fluid*. PhD thesis, Universtity of Birmingham, Birmingham, UK

Ozaki R, Nagao T (2004) Verification of seismic stability of caisson type breakwater. In: Proceedings of the 13th world conference on earthquake engineering. Paper no. 0588

Sugano T, Kaneko H, Yamamoto S (1999) Damage to port and harbor facilities. The 1999 Ji-Ji earthquake, taiwan, investigation into the damage to civil engineering structures. In: Japan Society of Civil Engineers, chap 5, pp 51–57

Sumer BM, Ansal A, Cetin KO, Damgaard J, Gunbak AR, Hansen NEO, Sawicki A, Synolakis CE, Yalciner AC, Yuksel Y, Zen K (2007) Earthquake-induced liquefaction around marine structures. J Waterw Port Coast Ocean Eng 133(1):55–82

Sumer BM, Kaya A, Hansen ONE (2002) Impact of liquefaction on coastal structures in the 1999 Kocaeli, Turkey earthquake. In: Proceedings of the international offshore and polar engineering conference, vol 12, pp 504–511

Tsai CP, Lee TL (1995) Standing wave induced pore pressure in a porous seabed. Ocean Eng 22(6):505–517

Westergaard HM (1933) Water pressure on dams during earthquakes. Trans ASCE 98(2):418–433

Wyllie LA (1986) The chile earthquake of March 3, 1985. Earthq Spectra 2(2):293–371

Young Y, White J, Xiao H, Borja R (2009) Liquefaction potential of coastal slopes induced by solitary waves. Acta Geotechnica 4:17–34

Yuksel Y, Cetin KO, Ozguven O, Isik NS, Cevik E, Sumer BM (2004) Seismic response of a rubble mound breakwater in Turkey. Proc Inst Civ Eng Marit Eng 157(4):151–161

Zienkiewicz OC, Chan AHC, Pastor M, Schrefler BA, Shiomi T (1999) Computational geomechanics with special reference to earthquake engineering. Wiley, England

Zienkiewicz OC, Chang CT, Bettess P (1980) Drained, undrained, consolidating and dynamic behaviour assumptions in soils. Geotechnique 30(4):385–395